School of Mathematical
and Physical Sciences

University of Reading

Department of Mathematics and Statistics

Preprint MPS-2014-07

3 February 2014

Microscopic definition of polymer entanglements

by

Alexei E. Likhtman and M. Ponmurugan

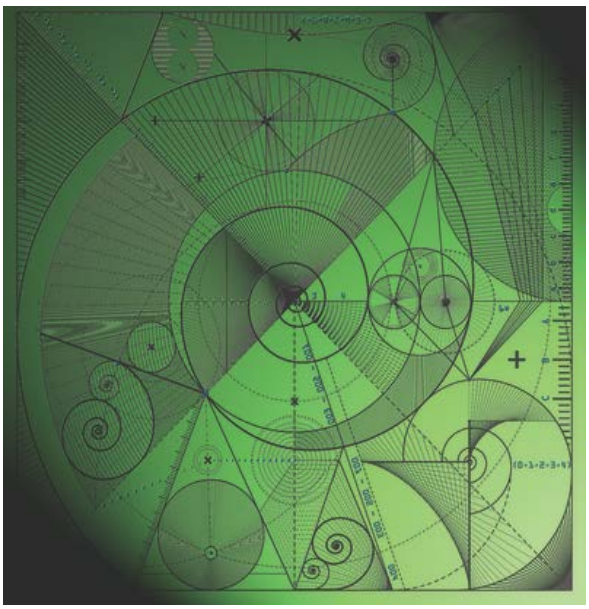

Microscopic definition of polymer entanglements

Alexei E. Likhtman, M. Ponmurugan*
School of Mathematical and Physical Sciences, University of Reading, Reading RG6 6AX, UK

February 3, 2014

Abstract

The dynamics of polymer melts and concentrated solutions is notoriously slow due to the fact that long polymer chains can not cross each other and therefore find themselves entangled. This popular belief is very difficult to quantify and convert into mathematical model because there is still no clear definition of what entanglement really is. In this paper we propose to define entanglement as a persistent contact between mean paths of the chains. In molecular dynamics (MD) simulations of well-entangled linear chains we discovered that such very tight and long-lived contacts exist in significant numbers. Moreover, once such contact is formed, it exists at every time step of the simulation until its destruction, which allows one to define its life time. We study several properties of individual entanglements and discover several unexpected features not taken into account in the tube theory or slip-links models. We believe that our simple and versatile definition opens the way to the truly microscopic understanding of polymer dynamics.

1 Introduction

This paper deals with the foundation of dynamical description of long polymer melts or concentrated solutions. It is well known that short polymer melts can be more or less described by the Rouse model, which approximates many chain problem of an interacting polymer melt by a single chain dynamics in an effective media. The single chain is modelled by a set of beads connected by linear springs, and the effect of all other chains on a particular chain is modelled by the random and friction forces. The random forces are delta-correlated in both space and time, and the friction forces obey the fluctuation-dissipation theorem. These assumptions allow one to write down precise equations of motion for the chain, and solve them exactly for almost all observables. These equations are the usual Langevin equations for the bead positions $\mathbf{R}_i$:

$$\zeta\frac{d\mathbf{R}_i}{dt} = -\frac{\partial U(\mathbf{R}_0...\mathbf{R}_N)}{\partial \mathbf{R}_i} + \mathbf{f}_i(t) \tag{1}$$

where $U(\mathbf{R}_0...\mathbf{R}_N)$ is the interaction potential between the beads, ζ is the bead friction, and $\mathbf{f}_i(t)$ is a random force acting on the bead i at time t. The random forces are governed by the fluctuation-dissipation theorem

$$\langle f_i^\alpha(t)\rangle = 0; \quad \left\langle f_i^\alpha(t) f_j^\beta(t')\right\rangle = 2k_BT\zeta\delta_{ij}\delta_{\alpha\beta}\delta(t-t') \tag{2}$$

where k_BT is the temperature multiplied by the Boltzmann constant, and α and β denote different Cartesian components. Three δ symbols here correspond to three decoupling assumptions: the random forces on different monomers along the chain are not correlated with each other, random forces in different directions are not correlated, and random forces at different moments of time are not correlated with each other. Finally, the interaction potential in Rouse model is given by a set of harmonic springs connecting neighboring monomers

$$U(\mathbf{R}_0...\mathbf{R}_N) = \frac{3k_BT}{b^2}\sum_{i=1}^{N}(\mathbf{R}_i - \mathbf{R}_{i-1})^2 \tag{3}$$

where b is the statistical segment length, and N in the number of bonds in the chain. An alternative and exactly equivalent equation of motion can be written in terms of stochastic differential equation using Ito calculus:

$$\zeta d\mathbf{R}_i = -\frac{\partial U(\mathbf{R}_0...\mathbf{R}_N)}{\partial \mathbf{R}_i}dt + \sqrt{2k_BT\zeta}d\mathbf{W}_i$$

*Current address: Department of Physics School of Basic and Applied Sciences, Central University of Tamilnadu Thiruvarur - 610 004, Tamilnadu, India.

where $\mathbf{W}_i$ are independent vector Wiener processes.

Despite the simplicity of such approximation, the Rouse model compares relatively well with molecular dynamics (MD) simulations [1],[2] and experiments [3],[4]. For example, the viscosity scales linearly with molecular weight and stress relaxation function scales as $G(t) \equiv \frac{V}{k_B T} \langle \sigma_{xy}(t)\sigma_{xy}(0) \rangle \sim t^{-1/2}$, where $\sigma_{\alpha\beta}$ is the stress tensor and V is volume.

The agreement with the Rouse model breaks dramatically when the molecular weight exceeds some critical value M_c. This is clearly observed in both MD and experiment. For example, the stress relaxation function $G(t)$ slows down and eventually develops a plateau, and the terminal time and viscosity start to grow with molecular weight as $N^{3.5}$ or so. These deviations from the Rouse model are generally believed to be caused by entanglements, or by the constraint that polymer chains can not cross each other. For long chain this constraint becomes significant and the effect of other chains on a probe chain can not be adequately described by the random and friction forces only. We then have a choice: either to modify equation 1, modify the potential 3 or random forces eq. 2, or to abandon eq.1 all together and write down new equations for another set of variables.

The tube theory follows the later choice: it postulates that for each chain there exists a curve in space (called a primitive path) such that on sufficiently long timescales the chain motion can be approximated by the one-dimensional motion along this primitive path. The equation of motion is then formulated for this one-dimensional motion, plus randomization of the primitive path at the ends when the chain leaves its tube. Notice a vague description of these main postulates as compared to the Rouse theory. The postulate about existence of the primitive path is not constructive, i.e. no definition is given in terms of the chain coordinates $\{\mathbf{R}_i\}$. But if one does not know how to construct the path, one can not unambiguously compare the tube theory predictions with the observation of chain coordinates from MD simulations. This situation has led to multiple and contradicting tube theories, but no single well defined model similar to the Rouse model exists. Besides that, there are numerous problems defining physical observables from the 1-d chain coordinates along the primitive path, as discussed in a recent book chapter[2].

Let's come back to the other possibility: can one modify eq.1 or it's ingredients, eqs.2 and 3, and have a consistent dynamics for the three-dimensional chain coordinates, which will adequately describe the motion along the primitive path? Since the effects of entanglements are caused by the other chains, it is clear that modification of interaction potential eq.3 will not be effective. It is also established that entanglements do not significantly affect the static properties of the chains, and thus the interaction potential should not be significantly different from the one used to model shorter unentangled chains. Thus, one should concentrate on modifying the forces from the environment, i.e. random and friction forces and perhaps some new forces. The choices again include anisotropic friction, random forces with memory and additional forces due to entanglements. The later choice seem to be most promising and it's the only one which is consistent with reptation at long lengthscales. Since the entanglements are supposed to confine the chain to a tube-like region, one comes to the natural conclusion that in order to model the effect of entangled matrix on a particular chain, *one has to introduce extra variables describing the environment.* These can be either tube or entanglements coordinates. For the modelling purposes, discrete notations are more convenient than the continuous, so we shall add a set of extra variables $\mathbf{a}_j$. One has to introduce some dynamics of these variables and some interaction or coupling between them and the chain variables. The simplest model which arises from this logic is the slip-spring model[5], which was shown to agree well with molecular dynamics simulations[6],[2]. The variables $\mathbf{a}_j$ in this model are the positions of the anchoring points, which are fixed in space but disappear when the chain end passes through a corresponding slip-link, and appear at the ends with a certain rate. There is also a set of one-dimensional positions of the slip-links along the chain x_j. The equations of motions are then very similar to the Rouse equation, but include one additional interaction term and an extra equation for new variables x_j

$$\zeta \frac{d\mathbf{R}_i}{dt} = -\frac{\partial U(\mathbf{R}_0 ... \mathbf{R}_N)}{\partial \mathbf{R}_i} + \mathbf{f}_i(t) - \frac{3k_B T}{N_s b^2}(\mathbf{R}_i - \mathbf{a}_j)\delta_{i,x_j}$$

where an extra term is non-zero only if the anchoring point j is connected to the monomer i. The equation for x_j can be either similar stochastic differential equation, or a master equation for jumps between the neighboring monomers, realized for example by the Metropolis algorithm. In both cases the evolution of x_j is governed by a well defined interaction potential between $\mathbf{a}_j$ and $\mathbf{R}_i$.

The slip-spring model is much more consistent and better defined than the tube model because the equations of motion for the chain coordinates are clearly specified and thus predictions for all experimental or simulation observables are readily available. However, the slip-spring model remains an empirical model in a sense that it postulates existence of the virtual objects (slip-links), which are not defined microscopically (i.e. from the positions of other chains), and thus their dynamics can not be verified in MD simulations. This becomes a serious problem when one wants to generalize the slip-spring model to fast deformations, branched polymers and other interesting situations. The aim of this paper is to identify entanglements in a multi-chain MD simulations and to study their dynamics. In section 2 we will define the mean paths consisting of the average positions of each bead over some time and will show that there are very persistent

contacts between the mean paths of different chains. *We will define entanglements as such persistent contacts between the mean paths.* Section 3 will introduce contact maps for chain pairs and a way to analyze such maps. In section 4 we will develop numerical algorithms to extract quantitative information about entanglements, and in section 5 we shall present the results of these algorithms applied to MD trajectories of well entangled chains. Section 6 will list the conclusions and the outlook.

2 Mean paths

It is clear that both entanglements and tube pictures predict existence of long lived contacts between different chains. However, it is not easy to detect such contacts. Indeed, in a usual modest simulation with $N_c = 100$ chains of length $N = 100$ for 10^7 time steps one has to process information about 10^{11} possible contacts even if the only information one is interested in is whether chain i is in contact with chain j or not. If one does process this information, one has to decide what to call a persistent contact. Chain positions are subject to rapid fluctuations and thus contacts between the chains appear and disappear rapidly. Thus, any analysis of such contact information is bound to be probabilistic, i.e. one can ask what is the probability of two chains to be in contact at time t providing they were in contact at time 0. One can not however assert whether these two contacts constitute the same entanglement or not. Such contact analysis was performed in ref.[7] for instantaneous chain coordinates. An approach based on an average interaction energy between non-bonded monomers was utilized in ref.[8] to visualize persistent contacts.

We note that contact probability information is not very useful to calibrate the tube or the slip-spring models. These models operate with survival probabilities, i.e. the probability that *the same* entanglement or tube segment exists at time t, if it was present in the system at time 0. In order to compute these probabilities, one has to track individual contacts and detect their appearance and disappearance.

In order to do that, we suggest to perform contact analysis on the mean paths $\hat{\mathbf{r}}_i$ rather than on the instantaneous chain coordinates $\mathbf{R}_i$. The mean paths were introduced in ref.[9] as

$$\hat{\mathbf{r}}_i(t) = \frac{1}{\tau_{av}} \int_{t-\tau_{av}}^{t} \mathbf{R}_i(t')dt'$$

i.e. they consists of the average positions of each bead over some averaging time τ_{av}. As was shown in ref.[9], the mean path of entangled polymer has a free energy of a semiflexible chain, i.e. the mean paths should be smooth on small length scales and of course follow the chain random walk on large scales. In this paper we report simulation results of 100 chains made of $N = 150$ beads, which are connected with finitely-extensible nonlinear (FENE) springs and interact with purely repulsive truncated Lennard-Jones potentials. Besides that, we add harmonic bending potential as described in ref.[10] with coefficient $k_b = 3$. This is done to create more entangled system relatively cheaply. The time step of the simulation is $\delta t = 0.012$, and the system was run for much longer than the longest relaxation time to ensure proper equilibration. According to the tube theory, the number of entanglements in our system is in the range of 7-15 depending on the definition, and the relaxation time of the strand between entanglements $\tau_e \approx 300 - 1000$. For mean paths, we will use $\tau_{av} = 1200$, or 10^5 timesteps, unless specified otherwise. We have also analyzed chains of different lengths and chains without bending potentials. However, for clarity and in the interest of space, we do not include these results unless they produce something qualitatively different from our $N = 150$ and $k_b = 3$ chains.

An instantaneous chain configuration is visually compared with the mean paths in Fig.1 (a) and (b).We see that the mean paths are smoother than the chains and fast fluctuations and small-scale wiggles are averaged out. Fig.1(b) illustrates that visually it is much easier to identify entangled chains by looking at their mean paths rather than at the instantaneous positions. If the averaging time is too large (i.e. 10^6 steps), than the local topology of mean paths is different from the topology of the chains. This is because the monomer motion on large scale is predominantly along the mean path. For example, if the chain moves along the circle of radius r, the mean path will make a smaller circle with the decreasing radius as the averaging time increases. Thus, we expect that with averaging the contacts will become more stable and well defined when the small fluctuations will be averaged out, but overaveraging will destroy some contacts. An algorithm for averaging over much longer times which avoids described artifacts is presented elsewhere[11]. To quantify the number of mean paths lying on top of each other (and thus violating topology) we plot interchain pair-distribution function $g(r)$ for the mean paths with different averaging time in Fig.2(b). For reference, Fig.2(a) shows all three pair distribution function for instantaneous positions. We see that for averaging time $\tau_{av} \leq 10^4$ steps, the probability for two mean paths to overlap is negligible, whereas for larger averaging times it is non-zero and topology is not preserved.

If one wants to preserve the topology but increase the averaging time further, one can use so called iso-configurational ensemble averaging[12]. One can start many short simulations from the same configuration but using different initial

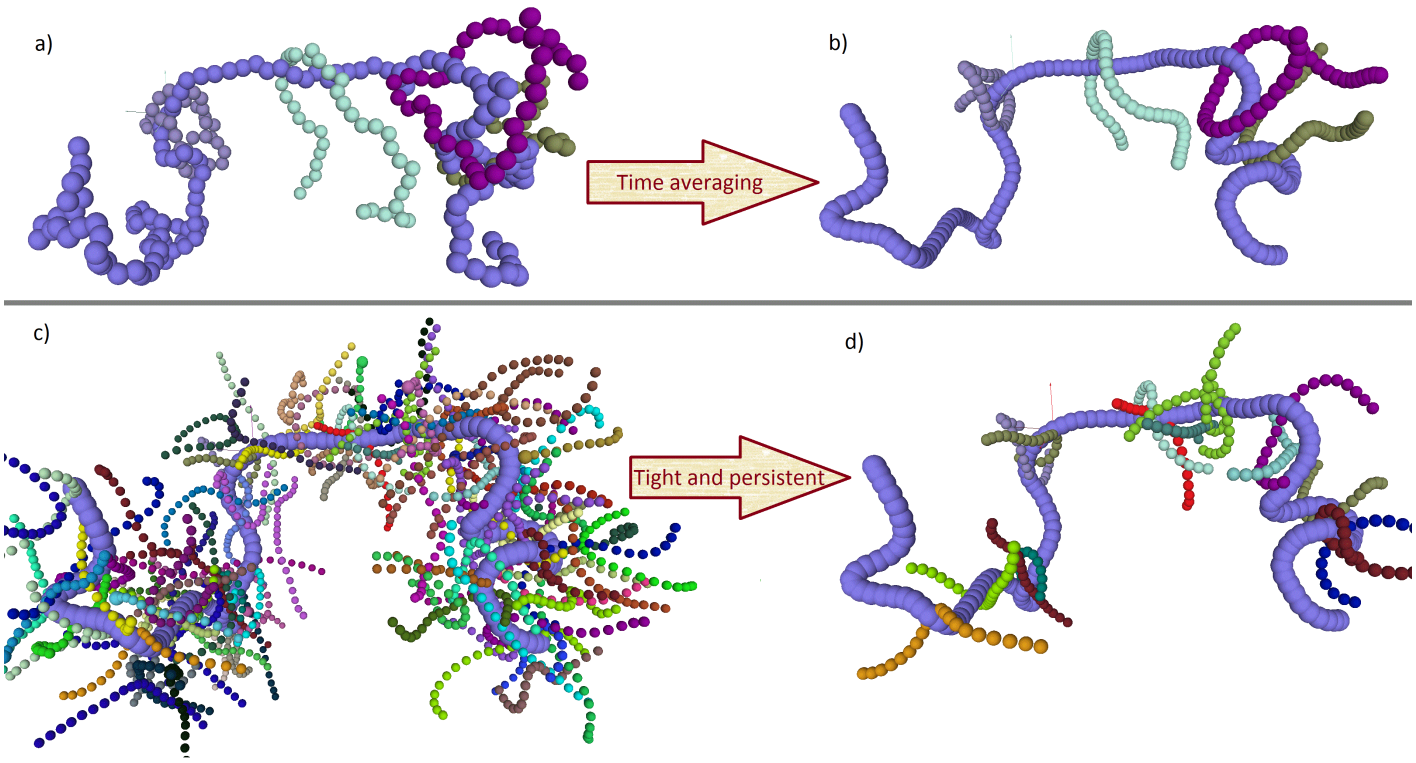

Figure 1: Illustration of mean path and contacts, for $N = 150, k_b = 3$ system. (a) Instantaneous positions of one chain and 4 pieces of other neighbor chains. (b) mean paths of the same chains. (c) Mean path of one chain with pieces of other mean paths which pass within distance 2σ of the selected chain. (d) Same but with only tight long-lived contacts ($q < 1.5$, $\tau > 10$)

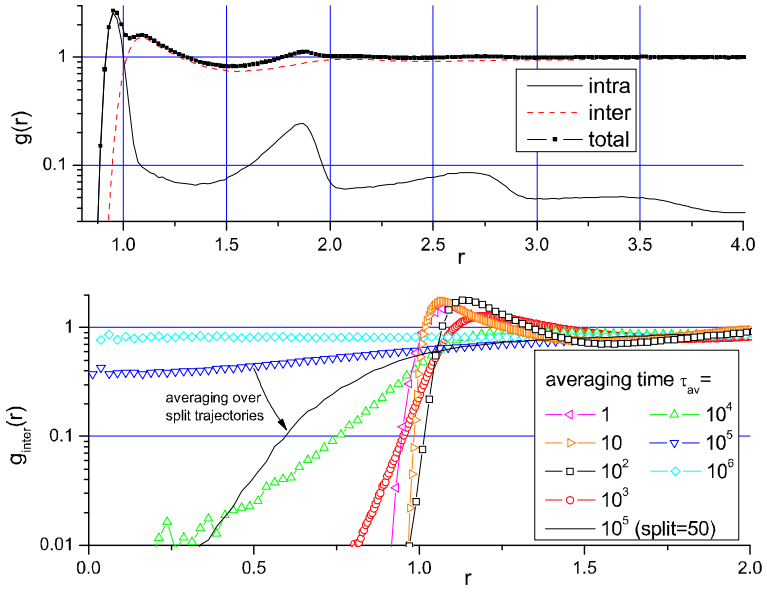

Figure 2: (a) Total, interchain and intrachain pair distribution functions for instantaneous monomer positions. (b) Interchain pair distribution function for mean paths with different averaging time, given in units of MD timestep $\delta t = 0.012$

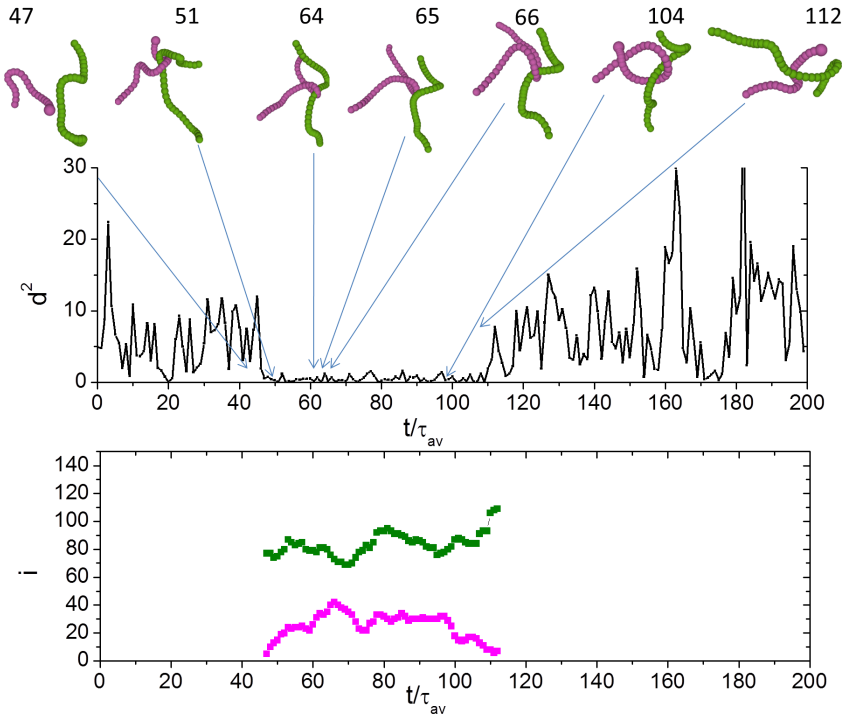

Figure 3: (a) Time evolution of the minimum distance between two chains — a tight contact is clearly idetifiable for time $47 < t/\tau_{av} < 112$. Corresponding pieces of mean paths are shown. (b) Monomers i_1 and i_2 participating in entanglement as a function of time.

velocities and/or random numbers of the thermostat. After running them for τ_{av}, the ensemble averaged mean path is obtained by averaging the mean paths from each simulation. As can be seen from Fig. 2(b, line), these paths do not lie on top of each other even for averaging times $\tau_{av} = 10^5$ steps, but do get closer to each other than 1 bead size σ. They also look smoother and entanglements are visually better resolved. A similar construction was used in ref.[13]. In this paper we will not use ensemble-averaged paths since it's much more expensive and does not bring significant advantages since our algorithms will not require topology preservation.

One is tempted to associate all contacts between the mean paths with entanglements. However, as Fig.1(c) illustrates, there are too many such contacts. Indeed, we showed all chains passing within a distance of 2σ from the selected chain — clearly there are much more contacts than the expected number of entanglements. Most of these contacts are very short lived, and thus probably irrelevant for slow dynamics. The majority of the short-lived contacts can be modelled by random and frictional forces. However, visualisation of time evolution of mean paths shows that there are very persistent contacts which also look like entanglements. We can illustrate this by plotting the minimum distance between two mean paths (with $\tau_{av} = 10^5$ steps) as a function of time. Fig.3(top) shows this distance $d^2_{\min}(j_1, j_2, t)$ defined as

$$d^2_{\min}(j_1, j_2, t) = \min_{i_1, i_2} (\hat{\mathbf{r}}_{i_1, j_1}(t) - \hat{\mathbf{r}}_{i_2, j_2}(t))^2 \tag{4}$$

where $\hat{r}_{i,j}$ is the mean position of monomer i of chain j.

We observe a very characteristic behavior: a very tight contact appears at around $t_b = 47\tau_{av}$ and disappears at $t_e = 112\tau_{av}$. Between these times, the average minimal distance between the two chains is very small (smaller than 1 σ^2 in this example), and it does not exceed $4\sigma^2$ at any time between t_b and t_e. In contrast, outside this time interval the minimal distance is much larger and fluctuates much stronger. In Fig.3 (bottom) we also show the monomers i_1 and i_2 corresponding to the minimum distance at each time. We notice that around creation and destruction time one of the monomers i_1 and i_2 is close to the end of the chain. This agrees very well with our mental picture of an entanglement: it has to be created and destroyed by one of the chain ends passing around the other chain (see however section 5.4 later for opposite examples). We also illustrated that the mean paths sometimes cross each other (in the frames $t/\tau_{av} = 64..66$), however this does not affect the minimal distance between them.

These observations give us a hope that long-lived contacts which look like entanglements do exist and can be quantified. However, the minimal distance alone as defined in eq.4 is not sufficient: indeed knowing that $d^2_{\min}(j_1, j_2, t)$ is small does not tell us how many entanglements exist between the chains j_1 and j_2. Thus, we should also resolve which monomers are in contact at which time. In order to do this, next section will introduce a notion of contact map.

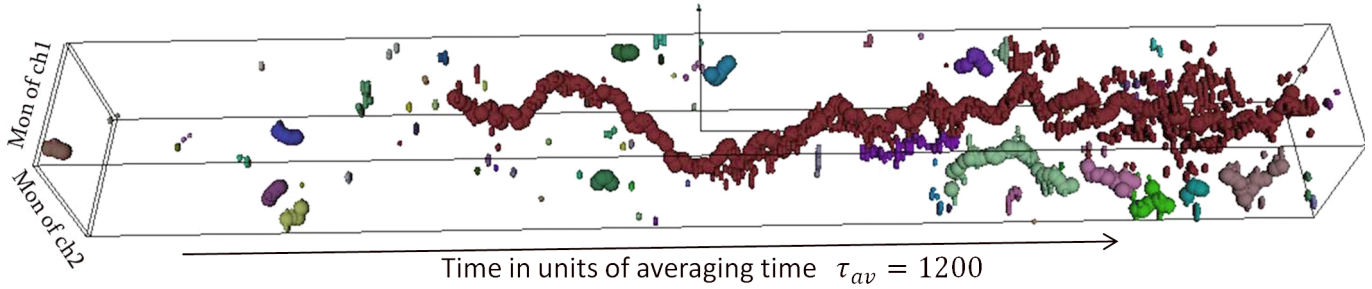

Figure 4: Contact map for a pair of chains. Different clusters are shown by different colours, one bigger sphere per time in each cluster show monomers participating in entanglement.

3 Contact maps

In order to quantify how many entanglements exist between a pair of chains as a function of time, we create a contact map. Each time the monomer i_1 of chain j_1 is within a certain distance d_{cut} of the monomer i_2 of chain j_2, we add a point (i_1, i_2, t) to a three-dimensional graph. For each pair of chains (j_1, j_2) in a simulation box we create such contact map, where we mark all mean monomers positions within certain distance of each other every τ_{av} along the horizontal time axis. An example of such contact map is shown in Fig.4, where we plot all contacts with distance $d^2 < 4$. We see that contacts can be grouped into clusters, each of which can be identified with a single entanglement. Moreover, the most important property of these clusters is that they are continuous in time, i.e. once an entanglement is created, it exists every time frame until it is destroyed. This allows us to separate clusters from each other, as shown by different colors in Fig.4. We say that two contacts belong to the same cluster if they are less than i_{cut} monomers apart along each chain and are in the adjacent or the same timeframe. We chose $i_{cut} = 20$, which we found to be a maximum number of monomers a chain can slide between the adjacent frames.

Even within each cluster, some time frames contain more than 1 contact. In order to be able to say which monomers are involved in an entanglement at a particular time, we develop an algorithm which processes each cluster of contacts and returns one monomer pair $i_1(t)$ and $i_2(t)$ for each time. We then calibrate this algorithm by looking at the mean paths configurations and verifying that an entanglement is near these monomers. We formulate the following requirements

- $i_1(t)$ and $i_2(t)$ should be continuous, and thus we should penalize large changes of these variables between consecutive moments of time.
- If we define the real-space position of an entanglement as

$$\mathbf{r}_e(t) = \frac{\hat{\mathbf{r}}(j_1, i_1(t)) + \hat{\mathbf{r}}(j_2, i_2(t))}{2}, \tag{5}$$

  it should also be continuous in time, i.e. we should penalize large entanglement jumps.
- we will assume that the long-lived entanglements are the most important ones. Thus, if the contact cluster branches, we shall select the longest branch.

We incorporate these requirements into a Dijkstra's algorithm of finding the shortest path on a graph [14]. For each cluster, we first select it's creation and destruction points. These are the contacts with the smallest and the largest time. We then compute the shortest path between these points. It should consist of one point at each time and the distance between the points at consecutive times is defined as

$$d^2(i_1, i_2, i_1', i_2') = (i_1 - i_1')^2 + (i_2 - i_2')^2 + C_l(\mathbf{r}_e(t) - \mathbf{r}_e(t+1))^2 \tag{6}$$

where $r_e(t)$ is the mid-point between two monomers participating in entanglement as defined by eq.5. Here (i_1, i_2) and (i_1', i_2') are monomers participating in an entanglement at times t and $t+1$ respectively. If there are several possible starting and finishing points of the contact cluster, we select the pair with the smallest distance. The coefficient C_l is the weighting of real space displacement as compared to the monomer-space displacements. The results are not very sensitive to it, and throughout the paper we set it to $5/\sigma^2$. Larger spheres in the contact map Fig.4 are the contacts selected by the shortest route algorithm, whereas all other contacts are shown by the smaller spheres.

Our contact map algorithm has three parameters: mean path averaging time τ_{av}, the cut-off distance which defines a contact d_{cut}, and the coefficient C_l in eq.6. The last parameter has only minor influence on determining the position of entanglements but not on the life time distribution or other important properties. In contrast, the first two parameters are very important and what we call an entanglement would depend on their choice.

4 Properties of individual entanglements

The algorithm of the previous section separates all contacts into clusters in monomer/time space. We now define and study the individual properties of these clusters which we shall call entanglements. There is clearly a multitude of such properties, and we select here just a few which seem to be correlated with the physical observations. The purpose of these properties is to separate essential entanglements, which determine long time dynamics, from the other short and random collisions.

First such property was already mentioned: it is the average of the minimum square distance between the monomers participating in the entanglements

$$q = \frac{1}{t_e - t_b + 1} \sum_{t=t_b}^{t_e} (\hat{\mathbf{r}}_{i_1,j_1}(t) - \hat{\mathbf{r}}_{i_2,j_2}(t))^2$$

where (j_1, i_1) and (j_2, i_2) are chain and monomer number participating in the entanglement at time t. If only one contact at each time exists, this quantity has a simple meaning of average square fluctuation in Fig.3 during the life of entanglement. As we show later, this property is the most effective characteristic of the entanglement strength, with strong entanglements corresponding to the small q. Since q characterizes the amount of fluctuations in the entanglement, which are facilitated by the slack in the two chains participating in it, we will call q an entanglement slack.

Intuitively, entanglements are associated with chains wrapping around each other. In topology, a linking number is used to describe linking between two closed curves. It is defined by the following double contour integral

$$l = \frac{1}{4\pi} \oint \oint \frac{\mathbf{r}_1 - \mathbf{r}_2}{|\mathbf{r}_1 - \mathbf{r}_2|^3} (d\mathbf{r}_1 \times d\mathbf{r}_2)$$

where $\times$ means a vector product, and the integration is over $\mathbf{r}_1$ and $\mathbf{r}_2$ running through all points along the two contours. For closed loops, this number is always an integer, and it is 0 if two loops are not linked (i.e. can be separated without cutting them). Although these properties are lost for open pieces of the chains, we found that it still contains information about how much the two chains are linked. We define a local linking number between the two pieces of chains as

$$l(t) = \frac{1}{4\pi} \sum_{k_1=i_1-\Delta i}^{i_1+\Delta i-1} \sum_{k_2=i_2-\Delta i}^{i_2+\Delta i-1} \mathbf{D}(\hat{\mathbf{r}}_{k_1,j_1}(t), \hat{\mathbf{r}}_{k_1+1,j_1}(t), \hat{\mathbf{r}}_{k_2,,j_2}(t), \hat{\mathbf{r}}_{k_2+1,j_2}(t)) \left[(\hat{\mathbf{r}}_{k_1+1,j_1}(t) - \hat{\mathbf{r}}_{k_1,j_1}(t)) \times (\hat{\mathbf{r}}_{k_2+1,j_2}(t) - \hat{\mathbf{r}}_{k_2,j_2}(t)) \right]$$

where

$$\mathbf{D}(\mathbf{r}_1, \mathbf{r}_2, \mathbf{r}_3, \mathbf{r}_4) = \frac{1}{(K+1)^2} \sum_{m=0}^{K} \sum_{n=0}^{K} \frac{\left(\mathbf{r}_1 + \frac{m}{K}(\mathbf{r}_2 - \mathbf{r}_1) - \mathbf{r}_3 - \frac{n}{K}(\mathbf{r}_4 - \mathbf{r}_3)\right)}{\left|\mathbf{r}_1 + \frac{m}{K}(\mathbf{r}_2 - \mathbf{r}_1) - \mathbf{r}_3 - \frac{n}{K}(\mathbf{r}_4 - \mathbf{r}_3)\right|^3}$$

Here we consider two pieces of chains having $2\Delta i + 1$ monomers (we will use $\Delta i = 10$ throughout the paper). The integral along each bond is approximated by the sums over $K + 1$ points. In practice we found that the simplest approximation with $K = 1$ works very well:

$$\mathbf{D}(\mathbf{r}_1, \mathbf{r}_2, \mathbf{r}_3, \mathbf{r}_4) \approx \frac{1}{4} \left(\frac{\mathbf{r}_1 - \mathbf{r}_3}{|\mathbf{r}_1 - \mathbf{r}_3|^3} + \frac{\mathbf{r}_1 - \mathbf{r}_4}{|\mathbf{r}_1 - \mathbf{r}_4|^3} + \frac{\mathbf{r}_2 - \mathbf{r}_3}{|\mathbf{r}_2 - \mathbf{r}_3|^3} + \frac{\mathbf{r}_2 - \mathbf{r}_4}{|\mathbf{r}_2 - \mathbf{r}_4|^3} \right)$$

We verified that entanglements with the high local linking number intuitively look right, which gives us hope that they will not appear and disappear frequently, but will be stable and long-lived. As discussed before, mean paths do not strictly preserve the topology, and therefore at some times the mean paths can be in a wrong topological state. We thus expect occasional strong fluctuations in the local linking number. This is indeed seen in Fig.5, where we plotted local linking number as a function of time for the same entanglement as shown in Fig.3. We see that about 25% of points are scattered around zero, whereas the rest are scattered around 0.84. Calculating the average linking number by averaging all the points does not make sense in this situation. Instead, we perform clustering analysis of the data using soft K-means algorithm assuming that the data are drawn from the sum of two Gaussian distributions[15]. If such clustering is successful, we define the average of the dominant cluster (0.84 in this case) as the local linking number of an entanglement.

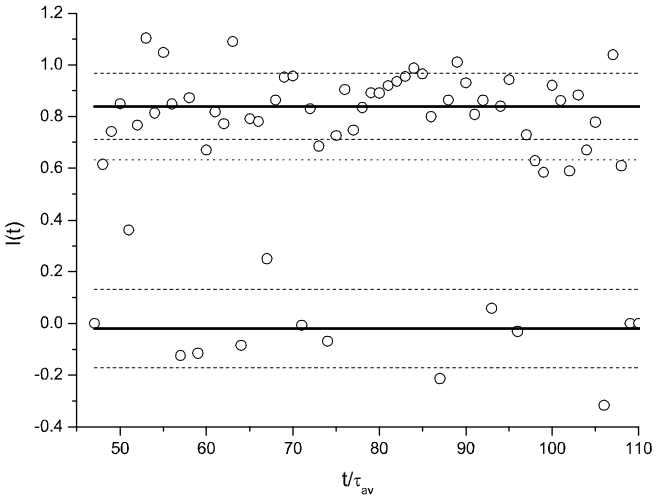

Figure 5: Time evolution of the local linking number for the same entanglement as in Fig.3.

With the definitions of entanglement slack and local linking number at hand, we can now investigate their probability distributions in a typical simulations. We perform contact map analysis with different cut-off distances for our chains with bending energy ($k_b = 3$), and for analogous system without bending potentials and with the similar number of entanglements ($N = 512$), and then compute the slack, life-time and local linking number of each contact cluster or entanglement. The slack distribution is shown for these two cases in Fig.6

We see that if all contacts are considered ($t_c = 1$), the slack distribution is very broad and decays only at cut-off $q = d_{cut}^2$, which is to be expected since no contact cluster can have slack larger than d_{cut}^2 by definition of contact. This is especially clear from the middle and the bottom panels of Fig.6, where we compare the same simulation analyzed with the different cut-off values. However if we consider only persistent contacts, i.e. contacts who live longer than a minimal time of t_c (measured in τ_{av} units), we see that the distribution narrows down significantly, and it is very sharply peaked around the most probable value, which is system and d_{cut} dependent. In case of flexible chains $k_b = 0$ we even observe a two-peaked distribution for $t_c = 20$, consisting of tight entanglements with $q \approx 6$ and weaker entanglements with $q \approx 8$. Varying t_c shows that long-lived entanglements do indeed have smaller slack. However this effect is not so easy to spot, and chains with bending potential do not show clear bimodal distribution at all.

In contrast, a clear bimodal distribution for chains with bending potential can be obtained in two-dimensional probability density of slack and local linking number $P(q, l)$, as plotted in Fig.7 for $k_b = 3$, $N = 150$ chain. We see that short-lived contacts with life-time $\tau < 50$ have small linking number and a slack with the maximum around $q = 2.5$. In contrast, long-lived entanglements have high linking number and small slack, with the maximum around $l \approx 0.65$ and $q \approx 1.4$. This plot represents clear evidence that long-lived persistent contacts have different properties as compared to short collisions. Since these tight persistent contacts are most likely candidates for entanglements, we now focus our attention on their properties.

To illustrate individual entanglements, we plot 25 randomly selected contacts with $q < 1.5$ and $\tau > 100$ at random time frame in Fig.8 (left). We see that many of them indeed have two mean paths wrapping around each other, but there are also some less obvious examples. We also see that the curvature of the mean paths is not directly correlated with the precence of another chain - this is a consequence of insufficient averaging. Additional iso-configurational averaging improves the pictures a little, as shown on the right. A much clearer picture is achieved with a new averaging algorithm published elsewhere[16], where we find very good correspondence between the curvature of the averaged path (called the tube axis) and the close contacts with other chains.

Another conclusion, which is obvious from the mean path visualization, is that all entanglements are very different from each other, even if only tight and long-lived ones are selected. This is illustrated in Fig.9, where we plotted all mean paths entangled with a particular pink mean path with entanglements with $q < 1.5$ and $\tau > 100$. To clarify the picture, we used ensemble average mean paths with 50 trajectories in the ensemble. It is obvious that different chains have different degrees of influence on the configuration of the pink chain. Whether such individuality of entanglements is important deserves further attention.

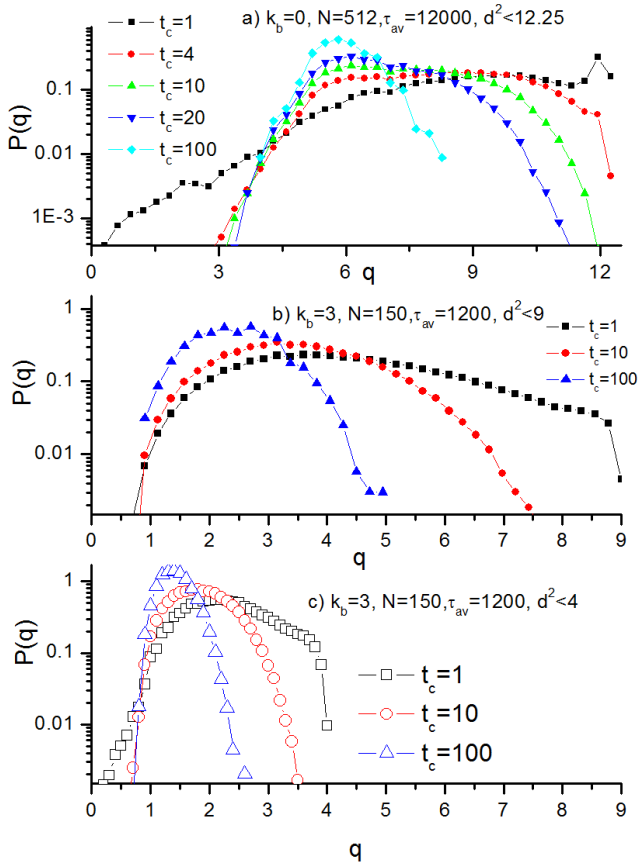

Figure 6: Entanglement slack distribution for contacts with different cut-off distance and chain stiffness and for different entanglement life times.

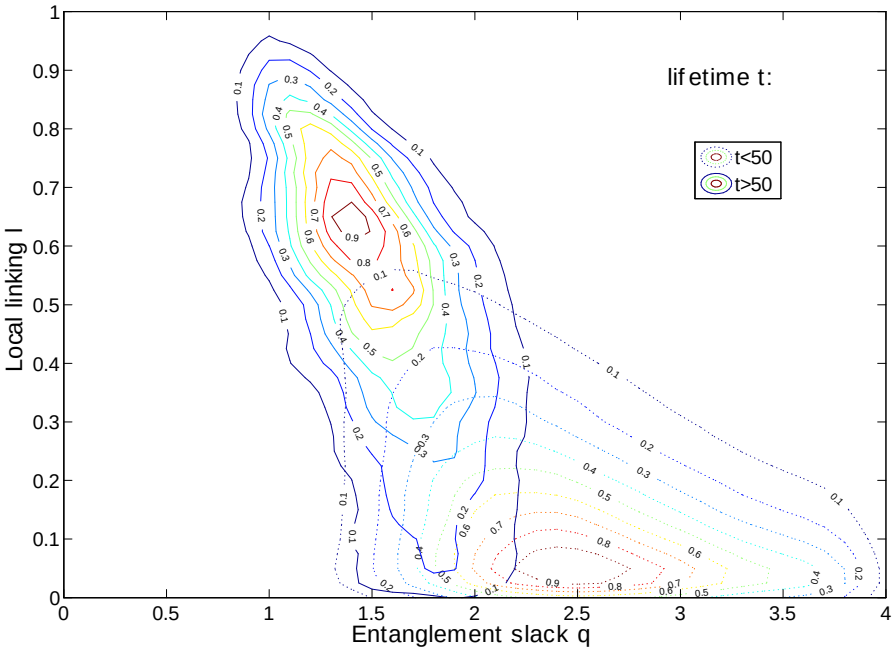

Figure 7: Probability density to find entanglements with certain slack and local linking number, normalized by the maximum density. Dashed lines show contour plot for all entanglements with lifetime smaller than $50\tau_{av}$, and solid lines — for entanglements with lifetime longer than $50\tau_{av}$.

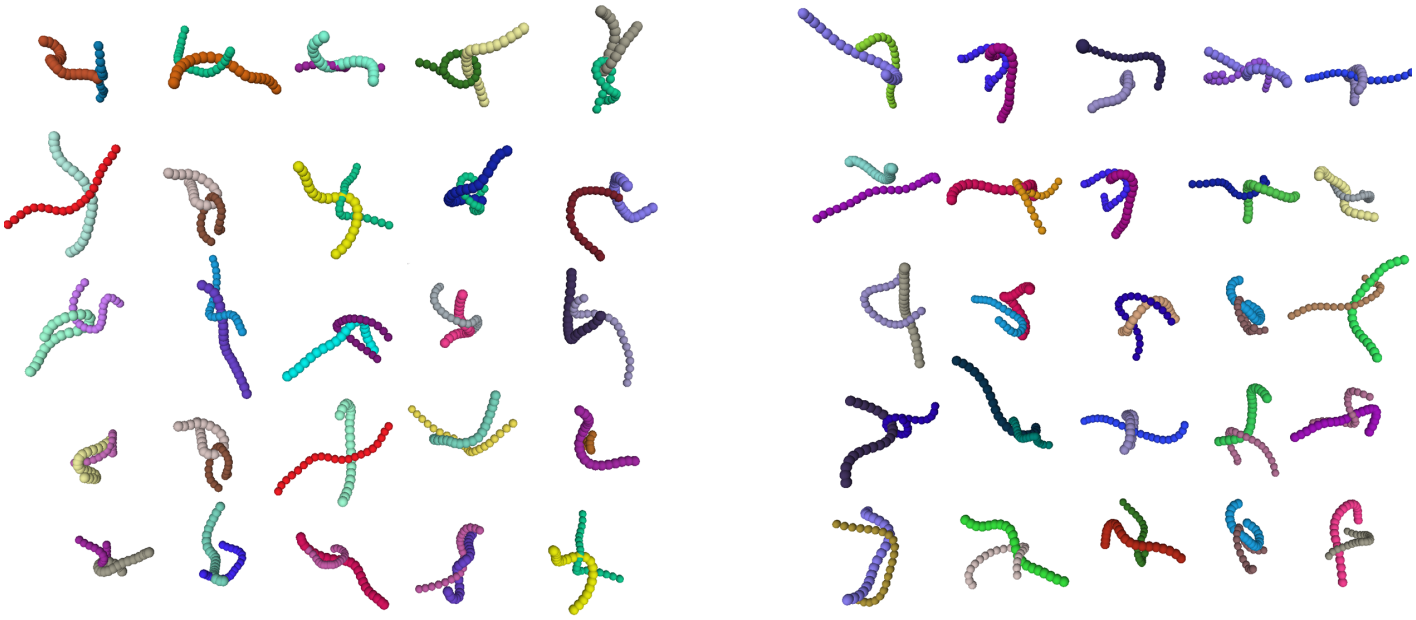

Figure 8: Left: Randomly selected entanglements with $q < 1.5$ and $\tau > 100$ at one moment of time for the mean path analysis. Right: the same from analysis of mean paths with configurational averaging over 50 trajectories, for $q < 2$ and $\tau > 50$.

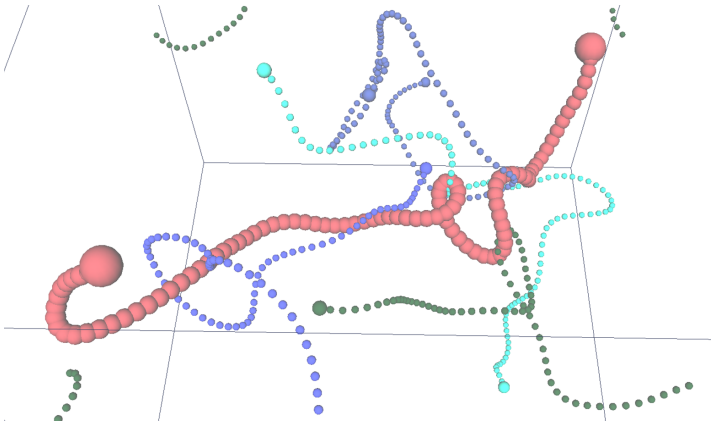

Figure 9: All mean paths entangled with the pink chain with tight longlived entanglements.

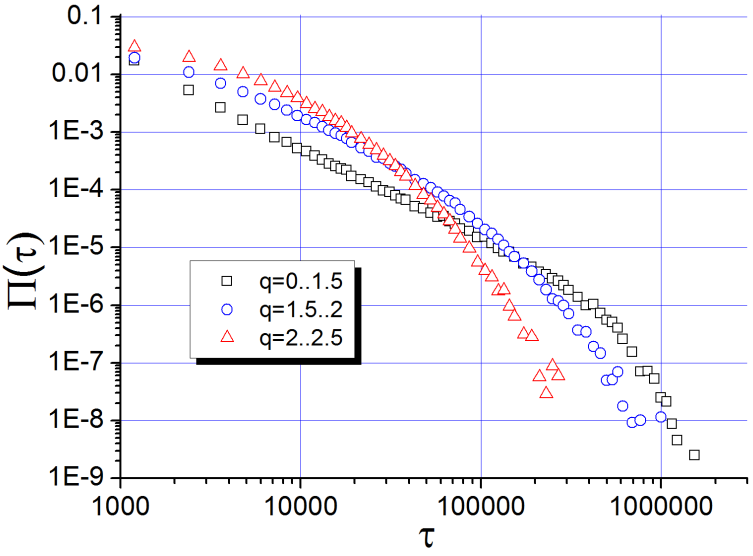

Figure 10: Probability density that a randomly selected entanglement within a certain slack range will have a lifetime τ.

5 Results and discussion

5.1 Entanglement survival probability

The persistence of contact clusters allow us to compute the lifetime of each entanglement, which is simply the length of each colored cluster in Fig.4 in horizontal direction. The easiest quantity to compute is the probability density of entanglement lifetime $\Pi(\tau)$. We created a list of all entanglements with different slack, pick an entanglement at random from this list and compute the probability density of it having a lifetime τ. The result is shown in Fig.10. The probability density decays rather quickly, which might lead to an erroneous conclusion that the long-lived entanglements are very rare. This is however not the distribution which is physically relevant. For stress, birefringence or dielectric relaxation, one is interested in the survival probability $P(t)$ that an entanglement picked at random from all entanglements which exist at time 0 will still exist at time t. It is easy to see that $P(t)$ is connected with $\Pi(\tau)$ with a simple relationship

$$P(t) = \frac{\int_t^\infty \Pi(\tau)(\tau - t)d\tau}{\int_0^\infty \Pi(\tau)\tau d\tau}$$

Indeed, the probability to pick up an entanglement which exists at a particular time is proportional to $\tau\Pi(\tau)$ (with appropriate normalization in denominator), and the probability of it surviving for time t is $\frac{\tau - t}{\tau}$ for $\tau > t$, thus the integration is performed over τ from t to infinity.

The resulting survival probability $P(t)$ is plotted in Fig.11 for entanglements with different slack, and compared with physical observables such as stress relaxation $G(t)$ (circles), end-to-end relaxation $\Phi(t)$ (triangles), and chain orientation tensor auto-correlation function $S_a(t)$ (squares). The chain orientation tensor is defined as [17],[2]

$$O_j^{\alpha\beta} = \frac{1}{N}\sum_{i=1}^{N}\left(R_{i,j}^{\alpha} - R_{i-1,j}^{\alpha}\right)\left(R_{i,j}^{\beta} - R_{i-1,j}^{\beta}\right)$$

where $R_{i,j}^{\alpha}$ is α-th Cartesian component of monomer i position on chain j. The autocorrelation $S_a(t)$ is then defined as

$$S_a(t) = \frac{1}{N_c}\sum_{j=1}^{N_c}\left\langle O_j^{\alpha\beta}(t)O_j^{\alpha\beta}(0)\right\rangle$$

where N_c is number of chains and we average over all off-diagonal components of the orientation tensor $\alpha \neq \beta$.

Physical observables were shifted vertically to be 1 at around $t = 1000$. This figure reveals a very interesting story. First, we see that tight entanglements ($q < 1.5$) survival function decays at a very similar time to the stress and orientation relaxation. This is in drastic contrast to entanglements with slightly higher slack, who seem to relax much

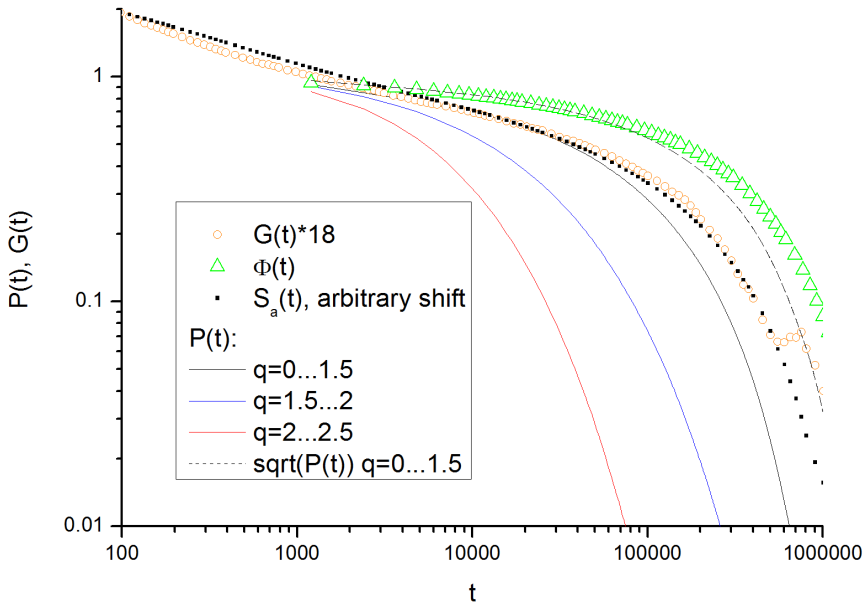

Figure 11: Entanglement survival probability function $P(t)$ compared with stress relaxation (circles), end-to-end relaxation (triangles) and orientation tensor auto-correlation (squares) functions.

faster. Note that according to Fig.6 there are very few entanglements with $q < 1$, so decreasing the q range further does not result in $P(t)$ being any closer to $G(t)$. According to the simple double reptation idea[18], the end-to-end relaxation should be slower than the stress relaxation, with approximate relation given by $\Phi(t) \sim \sqrt{G(t)}$. Indeed, we see that $\sqrt{P(t)}$ for tight entanglements agrees quite well with the end-to-end relaxation function. Finally, we notice that the agreement of $G(t)$ and $\Phi(t)$ with survival probability is not perfect: the physical observables relax about 30% slower than predicted by $P(t)$. This is not surprising since a simple tube picture assumes that once the entanglement disappears, the stress associated with it is relaxed immediately. In reality, the chain still needs some time to explore all available configurations. If during this exploration it is caught by another entanglement, this process is stopped again. Thus, predicting physical observables from entanglement survival probability remains a challenge for the future.

5.2 Entanglement density along the chain

We can now compute entanglement density $\rho_e(i)$ along the chain, which we define as the probability to find entanglement at monomer i at a particular moment of time. This is plotted in Fig.12 for entanglements of different slack and lifetime. The first striking feature of this figure is the higher density of entanglements near chain ends as compared to the middle of the chain. This however should not be so surprising if we remember that entanglements were defined as contacts between different chains, i.e. self-entanglements were neglected. The chain ends indeed have more contacts with other chains in comparison to the middle monomers because of excluded volume interactions. A middle monomer has two pieces of its own chain attached to it, which repel other chains. In contrast, the end monomer has only one such chain, which allows more other chains to approach it. This effect is however reduced for tight entanglements $q < 1.5$ (black squares), which do not show any maxima towards chain ends. This is likely to be caused by the fact that entanglements situated near chain ends have typically more slack, which partially cancels the effect explained above.

5.3 Tube segment survival function

The tube theory operates with the tube segment survival probability $\psi(s,t)$, which is defined as the probability for segment s to survive at least time t if it exists at time 0. Here s is a distance from the tube end along the tube contour. Doi and Edwards[19] postulated that if one neglects contour length fluctuations (CLF) and constraint release (CR), this function obeys a simple diffusion equation with absorbing boundary conditions at the ends, reflecting the fact that the tube segment dies if reached by either of the chain end. The solution of this equation is well known

$$\psi(s,t) = \frac{4}{\pi} \sum_{p,odd} \frac{1}{p} \sin\left(\frac{\pi p s}{L}\right) \exp\left(-\frac{p^2 t}{\tau_d}\right); \qquad \tau_d = \frac{L^2}{\pi^2 D_c} \tag{7}$$

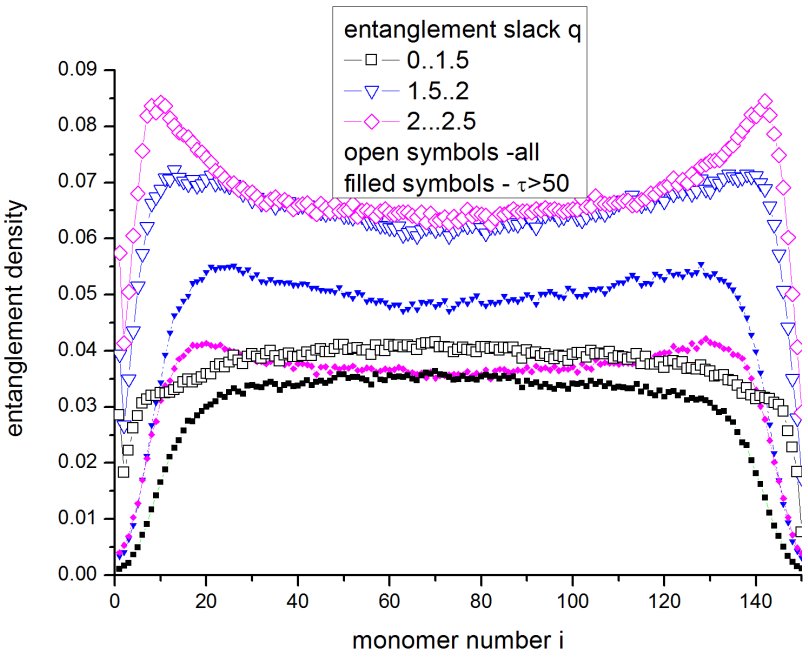

Figure 12: Entanglement density along the chain for different entanglement slack. Open symbols show all entnglements, whereas filled symbols - only entanglements with life time $\tau > 50$.

where the disentanglement time τ_d is the characteristic time of the longest mode, L is the tube length and D_c is center-of-mass diffusion coefficient along the tube (one-dimensional diffusion). Including CLF has two effects of $\psi(s,t)$ function. First, it will decrease significantly faster close to the ends of the tube. Second, the relaxation of the middle segments of the chain will still be described by eq.7, but with an effective tube length L_{eff}, which is reduced by CLF as compared to the original L.

We would like to compare and contrast entanglement survival probability with the tube survival probability. An entanglement in our definition is made by two chains, and therefore is characterized by two participating monomer indices. Thus, the meaningful survival probability of entanglement is a function of time and participating monomers on both chains $P(s_1, s_2, t)$, where $s_{1,2} = i_{1,2}/N$ and i_1 and i_2 are monomers of participating chains. Note that similar to the tube theory, s_1 and s_2 in the argument are the entanglement positions at time 0. This function is plotted in Fig.13 as determined from observing tight entanglements with $q < 1.5$.

The overall entanglement survival function $P(t)$ introduced earlier is obviously just an average of the monomer-resolved function

$$P(t) = \int_0^1 ds_1 \int_0^1 ds_2 P(s_1, s_2, t)$$

Note however that this formula is assuming a uniform entanglement density along the chain, which is slightly untrue near the chain ends (Fig.12).

To establish the connection of $P(s_1, s_2, t)$ with the tube survival probability, we assume that two chains participating in the entanglement move independently of each other, at least move independently along the tube, and at least on long timescales. This means that in order for entanglement to survive, neither of the chains should reach it with either of their ends. This assumption leads to a very simple relation

$$P(s_1, s_2, t) = \psi(s_1, t)\psi(s_2, t) \tag{8}$$

This means that $\psi(s,t)$ can be calculated from the measured $P(s_1, s_2, t)$ as

$$\psi(s,t) = \frac{\int_0^1 P(s, s', t)ds'}{\sqrt{\int_0^1 ds \int_0^1 ds' P(s, s', t)}}$$

The overall tube survival probability

$$\mu(t) = \int_0^1 \psi(s,t)ds$$

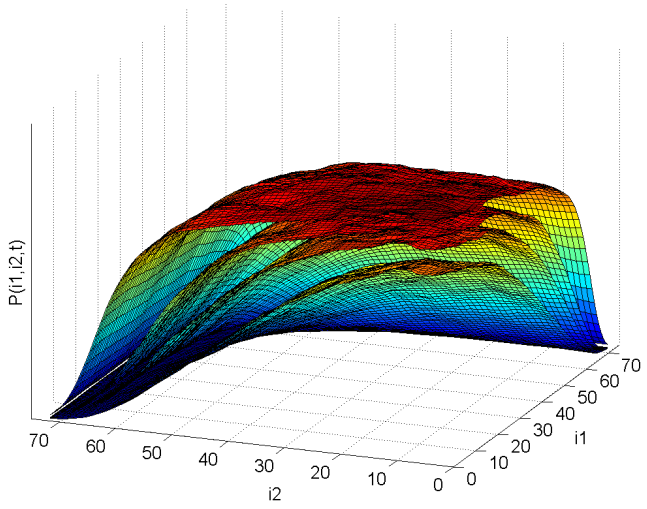

Figure 13: Entanglement survival probability for $t = 64, 128, 256, 512$ in units of $\tau_{av} = 1200$. The chain is $N = 150$ with bending energy $k_b = 3$.

is then simply given by

$$\mu(t) = \sqrt{P(t)}$$

which is what we used in Fig.11 (dashed line).

We followed this procedure and computed $\psi(s,t)$ for different times, and fitted them with Doi-Edwards expression eq.7, as shown in Fig.14. We have used two fitting parameters and successfully fitted all times simultaneously, excluding points with $|s-1/2| > 0.35$, which are affected by CLF and other end-effects. The fitting parameters were the terminal time τ_d and an effective tube length L_{eff}, and the obtained values are given in the Figure 14. The reptation time can be compared with the the longest relaxation time of the end-to-end vector (triangles in Fig.11) $\tau_\Phi = 4.7 \times 10^5$. Once again, end-to-end relaxation is slightly slower than the entanglement survival time.

We can also validate our assumption of independent reptation of two chains by predicting $P(s_1, s_2, t)$ from $\psi(s,t)$ using eq.8 and comparing it with the actual measured function. We performed such verification along the two lines in (s_1, s_2) plane, namely $s_1 = s_2$ and $s_2 = 1/2$, with results shown in Fig.15. We see that we can indeed recover the function of three variables $P(s_1, s_2, t)$ from the convoluted function of two variables $\psi(s,t)$.

One must comment on an unexpectedly large L_{eff} as compared to the predictions of the tube theory. Indeed, the tube theory assumes that the chain inside the tube behaves as a free Rouse chain stretched by the ends, with the same statistical segment as the unentangled chain in 3 dimensions. In the language of our recent paper[11], it assumes that $b_{1d} = b_{3d}$. In this case, the tube is predicted to be shortened by CLF[20],[21] as

$$\frac{L_{eff}}{L} = 1 - \frac{1.69}{\sqrt{Z}} + \frac{2}{Z} - \frac{1.24}{Z^{3/2}} + O\left(\frac{1}{Z^2}\right) \tag{9}$$

where $Z = N/N_e$ is called the number of entanglements. According to the tube theory, our chains must have $Z = 7..15$ entanglements, and therefore we expect $L_{eff}/L = 0.58..0.68$, i.e. the tube should appear shorter than the expected value without CLF by 30 or 40%. This is however not the case, and we only observe shortening by about 13%.

Several possible explanations of this effect spring to mind. First of all, as demonstrated in ref.[11], the one-dimensional statistical segment inside the tube b_{1d} can be different from its three dimensional counterpart. Smaller b_{1d} will result in reduction of the CLF effect. In particular this is to be expected for the slightly semi-flexible chains analyzed here. Another reason for weakening of the effect of CLF can be higher entanglement density near chain ends, which acts against CLF. More systematic investigation is required on this subject.

5.4 Creation/destruction of entanglements

According to the tube concept, entanglements can be created or destroyed by the chain ends. For example, to destroy an entanglement, one of the chains must reptate in such a way that entanglement will slide off the chain. This suggests

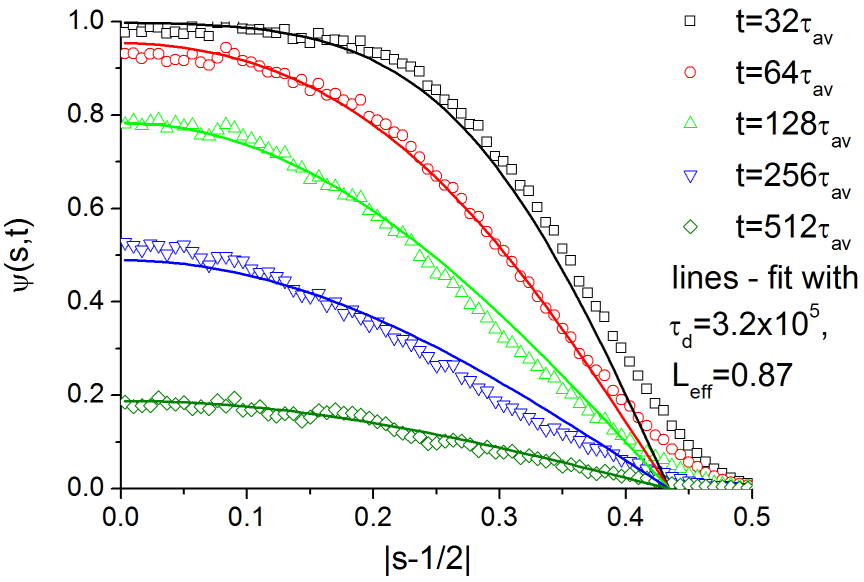

Figure 14: Tube survival probability extracted from the entanglement survival probability for 5 different times (symbols) compared to Doi-Edwards predictions with effective tube length.

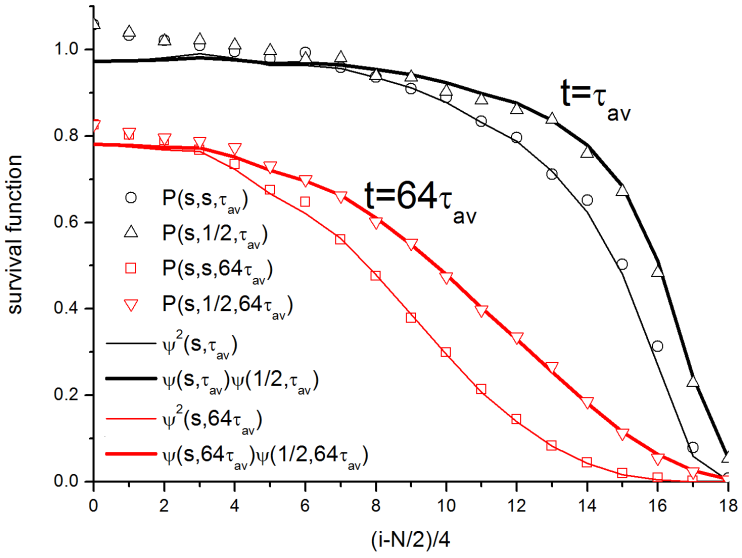

Figure 15: Entanglement survival probability along $s_1 = s_2$ and $s_2 = 1/2$ lines (symbols) compared with predictions obtained from $\psi(s,t)$ function (lines).

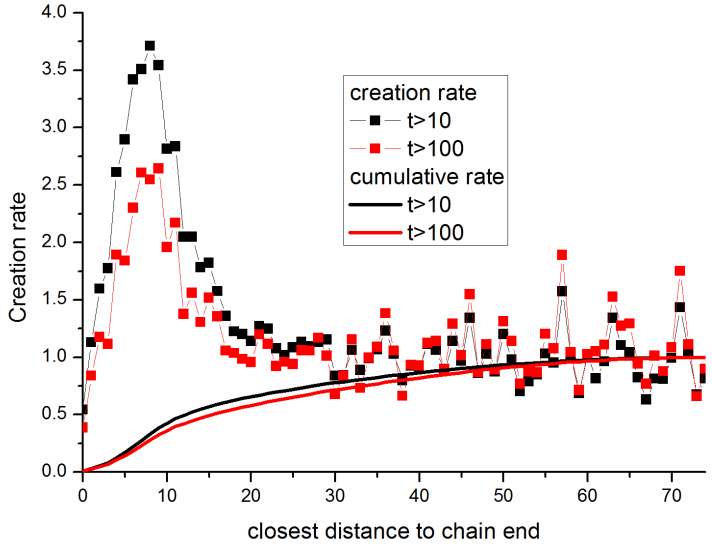

Figure 16: Closest distance to the chain end at the moment of entanglement creation.

that at the moment of entanglement destruction one of participating monomers s_1, s_2 must be close to either 0 or 1. The same is true for entanglement creation since we are talking about equilibrium time-reversible dynamics. Graphically, that means that in the contact map on Fig.4 the clusters must start and end close to the edges of (s_1, s_2) square. We test this assumption by computing the probability distribution of the closest monomer to the edge of unit square at the moment of creation or destruction of entanglements, as shown in Fig.16. In computing this probability density, we of course took into account that the area of the unit square with distance $x..x + dx$ to the nearest edge is a function of x. We normalize the results to be 1 far from the edge for ease of comparison.

We see that the creation probability is higher near the chain ends, but a significant number of entanglements are created far away from the chain ends. This is true even for long-lived entanglements $\tau > 100\tau_{av}$, as shown by red squares. The creation rate seem to be independent on monomer index for $i > 20$, thus we can say that all entanglements created further than 20 monomers away from any chain end are created in the middle of the chain. Cumulative probability curves (lines) show that there are about 40-50% of entanglements in our particular system which are created far from the chain ends (the percentage of course depends on the chain length). This means that either our definition of entanglement or entanglement creation is flawed, or the flaw lies in the tube theory assumption. The likely answer is that both are maybe to blame, and the likely cause of this observation are the multi-chain effects. Further investigations are needed to understand this effect.

5.5 Entanglement motion in space

Once entanglements are defined, one can also investigate their motion in real space. We define an entanglement position as an average of positions of two monomers participating in an entanglement, eq.5. We then select all entanglements who live longer than $200\tau_{av}$, and plot their mean-square displacement in space during their lifetime (green triangles in Fig.17). We also show here the same data for longer chains in order to illustrate the trend, where we selected entanglements who live even longer. For comparison, we plot the mean square displacement of the middle monomers of the same chains. We see that entanglements are not stationary in space even for very long chains of $N = 512$, and the volume it explores keeps growing. Since this plot is conditional on the entanglement to exist, this motion must be due to other entanglements appearing and disappearing in the vicinity. It can also be because of triple entanglements briefly analyzed in ref.[16]. Whether this process is important for stress relaxation or models of constraint release, and whether is has to be taken into account in the slip-springs model, deserves further investigation.

6 Conclusions

The main result of this paper is very clear observation of tight long-lived contacts between polymer chains in molecular dynamics simulations, which we propose to call entanglements. The key to this result is the analysis of contacts between the *mean paths*, composed from the mean positions of every monomer over time τ_{av}. We find that the contacts between two mean paths are very tight and persist for the time very close to reptation time of the whole chain. Moreover, these

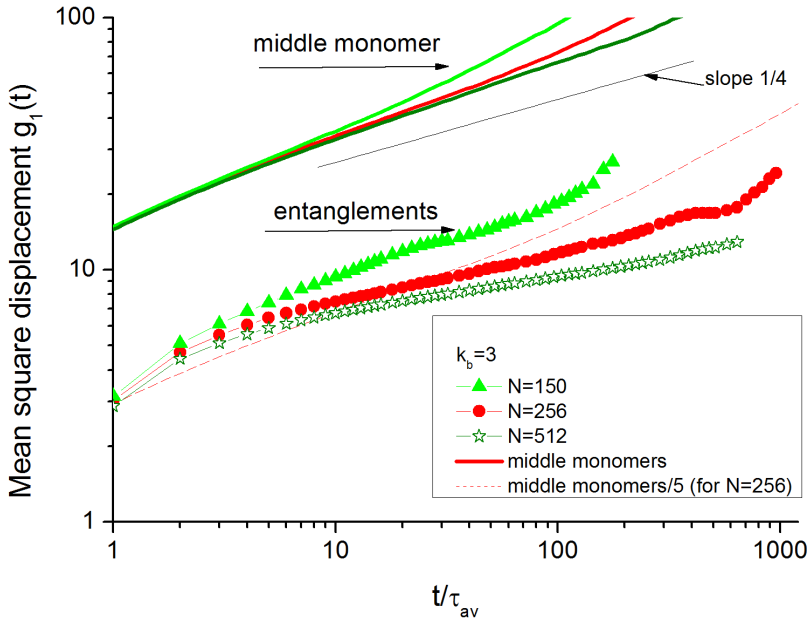

Figure 17: Mean square displacement of entanglement position in real space for chains with bending ($k_b = 3$) and different lengths. For comparison, the usual mean square displacement of the middle monomer is also shown.

long-lived contacts have high local linking number, and visually look very much like simple entanglements we imagine can happen between two ropes.

Motivated by these observations, we presented the first study of individual entanglements. We found that entanglement survival probability follows stress relaxation rather well, providing only tight entanglements are selected. We have also constructed tube survival probability, which fits well with reptation theory. There are however a few surprising observations which require further study. We found that entanglement density near the chain ends is higher than in the middle of the chain, which is a consequence of excluded volume interactions. We have also observed that contour length fluctuations are less efficient than predicted by the tube model. Although many entanglements are created by the chain ends, there is also a significant fraction of entanglements created far away from the ends of two participating chains. And finally, entanglements which exist for about reptation time, are moving in the volume which is increasing with time. These observation require separate detailed study, which should determine whether they need to be incorporated into the tube or slip-spring models.

A word of caution must be added concerning the number of entanglements. In the last 10 years there was a significant effort to find a single number N_e, which is the main parameter of the tube theory[22],[23],[24],[25]. Many competing definition were given and more and more advanced algorithms are being proposed to measure this number in MD simulations. We note that these efforts are only meaningful if the tube theory is valid, and if it is indeed a one parameter theory. If this would be true, it would be very easy to validate the methods of obtaining N_e: one would expect that simply substituting measured N_e into the tube theory one should be able to predict all observables measured in MD. This is however almost never attempted or at least never reported, simply because no such one-parameter tube theory exists. In recent publications, we described several limitations of the tube theory and argued that its detailed quantitative comparison with MD is quite meaningless at this stage[11], [2].

In such situation we do not think that determining number of entanglements or N_e is a well defined task worth pursuing. Instead, one must search for a better model and then seek to determine its parameters from MD. The slip-spring model[5] seem to be a reasonable candidate, and this paper aims to inform slip-spring model by studying behavior and properties of individual entanglements, which can be potentially modelled by the slip-springs. This is a subject of our next paper. Here we just note that the number of tight contacts depends strongly on the cut-off distance d_{cut}, average entanglement slack q, and the smallest lifetime of an entanglement. Although some reasonable choices can be made with some plausible qualitative arguments, this is not good enough for quantitative modelling.

The tube theory uses the tube length L and the chain end-to-end vector R_{ee} to define its main parameters $a \equiv \langle R_{ee}^2 \rangle / L$ and $Z = L^2 / \langle R_{ee}^2 \rangle$, which are often called tube diameter and the number of entanglements respectively. Both names are confusing and often misinterpreted. The parameter a has nothing to do with the fluctuations of the chain perpendicular to the tube (as the name suggests), but rather describes the tube properties along its contour. Thus,

a better name would be the tube Kuhns step. Indeed, the Kuhn step is defined in exactly the way a is defined. In turn, Z is then a number of tube Kuhn steps. The physical meaning of a and Z are the following: if we construct a freely jointed chain with the same contour length and the same average square end-to-end distance, this equivalent chain must have Z steps of length a. Note that this definition does not assume that the tube is a freely-jointed chain. Interpreting tube theory equations in this precise manner shows that the number of entanglements, however we choose to define them in microscopic simulations, does not have to be equal to Z as defined by the tube theory.

Acknowledgement. We thank Tim Palmer, Jing Cao and Daniel Read for constructive discussions and collaboration prior to this work. The bulk of this work was done in 2008-2010, supported by Engineering and Physical Sciences Research Council (EPSRC), UK trough Microscale Polymer processing consortium, with main definitions and results presented at several conferences[26]. Later this work was partially supported by the EPSRC grant H5094900.

References

[1] H. Meyer, *et al.*, *European Polymer Journal E* **26**, 25 (2008).

[2] A. E. Likhtman, *Polymer Science:A Comprehensive Reference* (Elsevier B.V., 2012), vol. 1, pp. 133–179.

[3] D. Richter, *et al.*, *Macromolecules* **27**, 7437 (1994).

[4] M. Rubinstein, R. H. Colby, *Polymer Physics* (Oxford University Press, 2003).

[5] A. E. Likhtman, *Macromolecules* **38**, 6128 (2005).

[6] S. K. Sukumaran, A. Likhtman, *Macromolecules* **42**, 4300 (2009).

[7] E. Ben-Naim, G. S. Grest, T. A. Witten, A. R. C. Baljon, *Phys. Rev. E* **53**, 1816 (1996).

[8] R. Yamamoto, A. Onuki, *Phys. Rev. E* **70**, 41801 (2004).

[9] D. J. Read, K. Jagannathan, A. E. Likhtman, *Macromolecules* **41**, 6843 (2008).

[10] A. E. Likhtman, S. K. Sukumaran, J. Ramirez, *Macromolecules* **40**, 6748 (2007).

[11] A. E. Likhtman, M. S. Talib, B. Vorselaars, J. Ramirez, *Macromolecules* **46**, 1187 (2013).

[12] A. Widmer-Cooper, P. Harrowell, H. Fynewever, *Physical Review Letters* **93**, 135701 (2004).

[13] W. Bisbee, J. Qin, S. T. Milner, *Macromolecules* **44**, 8972 (2011).

[14] E. W. Dijkstra, *Numerische Mathematik* **1**, 269 (1959).

[15] D. J. MacKay, *Information Theory, Inference, and Learning Algorithms* (Cambridge University Press, 2003).

[16] A. E. Likhtman, *Soft Matter, submitted* (2013).

[17] J. Cao, A. E. Likhtman, *Phys. Rev. Lett.* **104** (2010).

[18] C. Tsenoglou, *Polymer* pp. 1762–1767 (1991).

[19] M. Doi, S. F. Edwards, *The theory of polymer dynamics* (Clarendon Press, New York, USA, 1986).

[20] M. Doi, *J. of Polym. Sci.* **21**, 667 (1983).

[21] A. E. Likhtman, T. C. B. McLeish, *Macromolecules* **35**, 6332 (2002).

[22] R. Everaers, *et al.*, *Science* **303**, 823 (2004).

[23] C. Tzoumanekas, D. N. Theodorou, *Macromolecules* **39**, 4592 (2006).

[24] R. S. Hoy, K. Foteinopoulou, M. Kroger, *Phys. Rev. E* **80**, 031803 (2009).

[25] J. Qin, S. T. Milner, *Soft Matter* **7**, 10676 (2011).

[26] A. E. Likhtman, *"Microscopic definition of Entanglement", March APS meeting, Portland, Oregon, 2010; Society of Rheology Annual Meeting, Santa Fe, New Mexico, 2010;*.

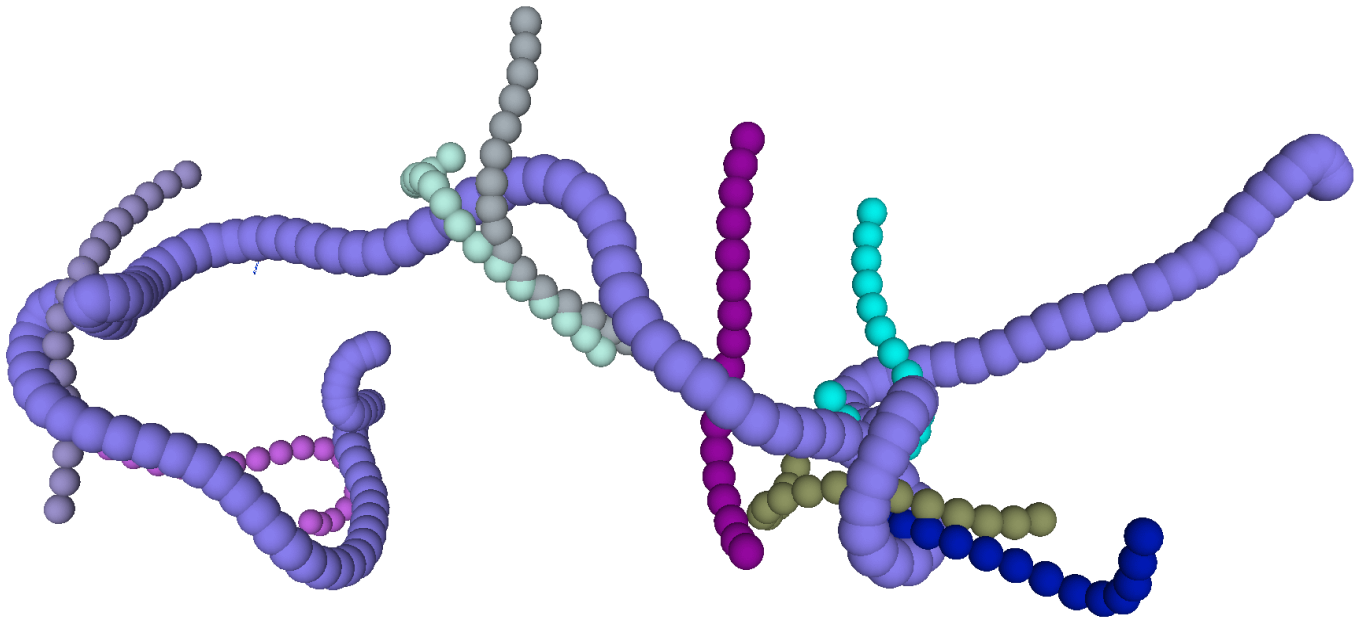

Table of contents figure
"Microscopic definition of polymer entanglements" *Alexei E. Likhtman, M. Ponmurugan*